Eddy-current evaluation of 3-D defects in a metal plate: a first analysis of a contrast-source gradient method

Daniel Dos Reis, Marc Lambert, Dominique Lesselier

Eddy-current evaluation of 3-D defects in a metal plate: a first analysis of a contrast-source gradient method

D. Dos Reis, M. Lambert, D. Lesselier
Département de Recherche en Électromagnétisme – Laboratoire des Signaux et Systèmes
CNRS-SUPÉLEC-UPS, Plateau de Moulon, 3 rue Joliot Curie,
91192 Gif-sur-Yvette Cedex, France, http://www.lss.supelec.fr

Abstract Retrieval of voluminous defects in a non-magnetic metal plate from maps of time-harmonic anomalous magnetic fields in air due to a source nearby is performed by a contrast-source, gradient-type technique which uses the binary aspect of the sought conductivity distributions. The functional analysis within a vector integral formulation of the diffusive fields is sketched and the efficiency of the approach is discussed in the light of preliminary inversion results obtained with synthetic data.

1 Introduction

We investigate the evaluation of 3-D bounded (voluminous) defects of known conductivity (voids, inclusions) inside a flat, horizontal non-magnetic metal plate from anomalous magnetic fields observed when a low-frequency source is operated nearby. The source consists of an air-core coil probe positioned above the expectedly damaged zone. The data consist of a 2-D map of one single component (the vertical one) or of all three components of the anomalous magnetic field at discrete locations in a planar surface above the plate.

Our main aim is not to introduce fully novel modeling tools of, and solution methods to, that demanding 3-D shape inversion problem, but to study whether one could tackle this problem by combining a number of recently introduced methods, when as now the embedding environment is a planar (conductive) layer, when the scatterers are three-dimensionally bounded, when illumination and observation are made from above the layer (aspect-limited data), and even when a single component of the vector magnetic field is collected on a limited, coarse mesh. These methods have been developed in order

- to calculate the eddy-current pattern in a planarly-layered conductive environment affected by a localized inhomogeneity of arbitrary geometry using exact solutions as well as extended-Born approximations developed within a rigorous, *full-wave* vector domain integral formulation of the diffusive fields inside and outside the affected sample [1, 2];

- to extract the distribution of conductivity of a 3-D, possibly multiply-connected voluminous object buried in an infinite conductive space from a magnetic field observed nearby, using a contrast-source-based gradient-type method [3, 4] in an Earth's subsurface imaging context;

- to use the prior information that the sought defects are of prescribed conductivity contrast with respect to their environment, their 3-D maps ideally consisting of distributions of black and white voxels (in the exterior and in the interior of the defects) as is the case already in [5] and as it has been much studied in 2-D geometries since the early approach [6] of binary-specialized modified gradient methods.

Previous investigations [1, 2] have shown that anomalous magnetic fields are modeled with fair accuracy –in manageable computational time on a standard work-station– by the aforementioned integral formulation, and we do not come back to this topic here. We mostly outline below how this *hybrid* inversion method can be properly developed, and give a few typical results. Test cases at this still preliminary stage come from synthetic data calculated on canonical 3-D models of mm-sized parallelepipeded void defects in an Inconel 600 plate probed in the 150 – 300 kHz frequency range.

2 The algorithm

Let us refer to the configuration sketched in Fig. 1. A possibly multiply-connected 3-D defect Ω of constant conductivity σ (it will be 0 in the numerical examples) is embedded within a non-magnetic linear isotropic metal plate of conductivity σ_2. Eddy currents are generated in the plate using a time-harmonic (circular frequency ω, time-dependence $\exp\left(-\mathrm{j}\omega t\right)$) coil source carrying electrical currents J_C at fixed location in air (permeability μ_0, permittivity ϵ_0). Perturbation of the eddy current pattern produces an anomalous magnetic field that is observed in a prescribed planar surface $\mathcal{S}$ in air.

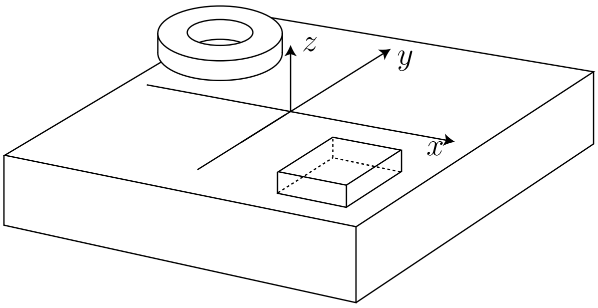

Figure 1: Configuration of study: a pancake-type source probe is set at fixed location above the damaged metal plate, here sketched as a void parallelepiped, the time-harmonic magnetic field being sampled in a plane of observation at fixed height above the plate.

The electromagnetic field $\mathbf{E}, \mathbf{H}$ at any $\mathbf{r}$ in the plate (corresponding quantities will be marked by subscript 2) and in air (using subscript 1 if above the plate, and 3 if below) are cast into a rigorous vector domain (contrast-source) integral formulation from application of the Green theorem onto the quasi-static Maxwell's PDE –involving the Green dyads of the layered environment. So, the field modeling requires the calculation of a fictitious contrast source $\mathbf{J}_2\left(\mathbf{r}\right) = \sigma_2 \chi\left(\mathbf{r}\right) \mathbf{E}_2\left(\mathbf{r}\right)$, where $\chi\left(\mathbf{r}\right)$, equal to 0 outside Ω and to $\chi_c = \sigma/\sigma_2 - 1$ inside Ω, is the electrical contrast between the metal and the defect Ω (for a void, $\chi_c = -1$). For any $\mathbf{r}$ in Ω,

$$\mathbf{J}_2\left(\mathbf{r}\right) = \mathbf{J}_{20}\left(\mathbf{r}\right) + \mathrm{j}\omega\mu_0\sigma_2\chi\left(\mathbf{r}\right) \int_\Omega \underline{\mathbf{G}}_{i2}^{ee}\left(\mathbf{r}, \mathbf{r}'\right) \mathbf{J}_2\left(\mathbf{r}'\right) d\mathbf{r}', \tag{1}$$

whilst the anomalous magnetic field $\mathbf{H}_1^{\mathcal{S}}$ in $\mathcal{S}$ follows from

$$\mathbf{H}_1^{\mathcal{S}}(\mathbf{r}) = \int_{\Omega} \underline{\mathbf{G}}_{12}^{me}(\mathbf{r}, \mathbf{r}')\, \mathbf{J}_2(\mathbf{r}')\, d\mathbf{r}'. \tag{2}$$

In the above $\mathbf{J}_{20} = \sigma_2 \chi \mathbf{E}_{20}$, where $\mathbf{E}_{20}(\mathbf{r}) = \mathrm{j}\omega\mu_0 \int_{\mathcal{S}} \underline{\mathbf{G}}_{21}^{ee}(\mathbf{r}, \mathbf{r}')\, \mathbf{J}_C(\mathbf{r}')\, d\mathbf{r}'$ represents primary currents associated to the electrical current $\mathbf{J}_C$ in the coil source C in medium 1; $\underline{\mathbf{G}}_{ij}^{ee}(\mathbf{r}, \mathbf{r}')$ and $\underline{\mathbf{G}}_{ij}^{me}(\mathbf{r}, \mathbf{r}')$ are the electric-electric and magnetic-electric Green dyads made of the electric and magnetic fields at $\mathbf{r}$ in medium i due to a Dirac electrical current at $\mathbf{r}'$ in medium j, respectively.

Upon iteratively solving (1) by a Conjugate-Gradient Fast-Fourier-Transform Method of Moments using pre-calculated samples of the Green dyads the anomalous field follows from (2) (extended-Born approximations enabling us to bypass the solution of (1) via the introduction of a depolarization dyad independent of the field) [1, 2, 7]. Correspondingly, the inversion problem requires us to determine some conductivity contrast within each voxel of a prescribed 3-D box $\mathcal{D}$ containing the unknown defect of support Ω in order to produce an anomalous magnetic field close enough in some sense to data $\boldsymbol{\zeta}$ collected in $\mathcal{S}$, being assumed that the true distribution is binary.

As already indicated, binary-specialized modified gradient methods [5, 6] and contrast-source gradient-type methods [3, 4] have been investigated for nonlinearized wave field inversion. Lack of place precludes us to go into their respective machineries. Combining both methods by specializing the contrast-source approach to a binary contrast –in original fashion and with promising results as shown in section 3 by numerical experimentation– can be done as follows.

The formulation of interest is written into shorthand operator form using Green dyadic operators: $\underline{\mathcal{G}}_{22}^{ee}\, \mathbf{J}_2 = \mathrm{j}\,\omega\,\mu_0 \int_{\mathcal{D}} \underline{\mathbf{G}}_{22}^{ee}(\mathbf{r}, \mathbf{r}')\, \mathbf{J}_2(\mathbf{r}')\, d\mathbf{r}'$ and $\underline{\mathcal{G}}_{12}^{me}\, \mathbf{J}_2 = \int_{\mathcal{D}} \underline{\mathbf{G}}_{12}^{me}(\mathbf{r}, \mathbf{r}')\, \mathbf{J}_2(\mathbf{r}')\, d\mathbf{r}'$. Two equations are of interest: the data equation

$$\boldsymbol{\rho} = \boldsymbol{\zeta} - \underline{\mathcal{G}}_{12}^{me}\, \mathbf{J}_2^n \tag{3}$$

tells us that some contrast source $\mathbf{J}_2$ in $\mathcal{D}$ radiates a certain magnetic field in $\mathcal{S}$ whose discrepancy with data $\boldsymbol{\zeta}$ is measured by vector residual $\boldsymbol{\rho}^n$; the state equation

$$\boldsymbol{\epsilon} = \sigma_2\, \chi\, \mathbf{E}_2 - \mathbf{J}_2 \tag{4}$$

tells us that this contrast source is consistent with a contrast distribution χ (here, purely real) in $\mathcal{D}$, the degree of consistency being appraised by vector residual $\boldsymbol{\epsilon}$, letting $\mathbf{E}_2 = \mathbf{E}_{20} + \underline{\mathcal{G}}_{22}^{ee}\, \mathbf{J}_2$.

As for the sought binary aspect of the contrast distribution (valued to χ_c or to 0 at any $\mathbf{r}$ in $\mathcal{D}$), and in order to use gradient methods that require us to restore differentiability with respect to this distribution, it is enforced via the nonlinear transformation

$$\chi = \chi_c\, \Psi(\tau)\,, \Psi(\tau) = (1 + \exp\ (-\tau/\theta))^{-1}\,, \tag{5}$$

where θ is a strictly positive, real-valued tuning parameter which is controlling the slope of the strictly monotonous real function Ψ (bounded between 0 and 1 and varying from 0 to 1 when τ is increased), the $\mathbf{r}$-dependence being implied. In practice, decreasing θ yields an electrical contrast χ closer to χ_c (resp., to zero) for a given positive (resp., negative) τ at same $\mathbf{r}$.

The solution itself now relies on the construction of two sequences of τ^n and $\mathbf{J}_2^n$ (correspondingly, of $\mathbf{E}_2^n$) that are both function of space $\mathbf{r}$ (implied) in $\mathcal{D}$ –once chosen proper first guesses at $n = 1$– so as a suitable cost functional $\mathbf{F}$ is decreased from one iteration to the next. Using $\|.\|_{\mathcal{S}}$ and $\|.\|_{\mathcal{D}}$ as norms on $L_2(\mathcal{S})$ et $L_2(\mathcal{D})$ and (later on) corresponding scalar products $\langle , \rangle_{\mathcal{S}}$ and $\langle , \rangle_{\mathcal{D}}$, the general expression of $\mathbf{F}$ reads as

$$\mathbf{F} = \eta_{\mathcal{S}} \|\boldsymbol{\rho}\|_{\mathcal{S}}^2 + \eta_{\mathcal{D}} \|\boldsymbol{\epsilon}\|_{\mathcal{D}}^2 , \tag{6}$$

where weight $\eta_{\mathcal{S}} = \|\boldsymbol{\zeta}\|_{\mathcal{S}}^{-2}$ is constant for given data $\boldsymbol{\zeta}$ and where weight $\eta_{\mathcal{D}} = \|\sigma_2\, \chi\, \mathbf{E}_{20}\|_{\mathcal{D}}^2$ is contrast-dependent.

The determination of the contrast source $\mathbf{J}_2^n$ is carried out first. At iteration n, one simply chooses $\mathbf{J}_2^n = \mathbf{J}_2^{n-1} + \alpha^n \mathbf{v}^n$, where the complex-valued, $\mathbf{r}$-dependent (3-component) vector $\mathbf{v}^n$ is a conjugate-gradient direction of displacement of the Polak-Ribière type and where the complex-valued constant parameter α^n is a coefficient of displacement. One sets for $n > 1$

$$\mathbf{v}^n = \mathbf{g}^{v,n} + \frac{\langle \mathbf{g}^{v,n}, \mathbf{g}^{v,n} - \mathbf{g}^{v,n-1} \rangle_{\mathcal{D}}}{\langle \mathbf{g}^{v,n-1}, \mathbf{g}^{v,n-1} \rangle_{\mathcal{D}}} \tag{7}$$

(at $n = 1$, $\mathbf{v}^1 = \mathbf{g}^{v,1}$). $\mathbf{g}^{v,n}$ is the complex-valued gradient (Fréchet derivative) of $\mathbf{F}$ with respect to the contrast source $\mathbf{J}_2$ at $\mathbf{J}_2^{n-1}$, the contrast being kept fixed at χ^{n-1} in the calculation (i.e., τ^{n-1} is kept fixed). Formal derivation in $\mathbf{F}$ of the squared norms of the residuals that are given in operator form in (3) and (4) being carried out in line with earlier works, e.g., [3, 4, 5, 6] and many references therein, one can show that this gradient reads as

$$\mathbf{g}^{v,n} = -\eta_{\mathcal{S}}\, \underline{\mathcal{G}}_{12}^{me^*} \boldsymbol{\rho}^{n-1} - \eta_{\mathcal{D}}^{n-1} \left(\boldsymbol{\epsilon}^{n-1} - \underline{\mathcal{G}}_{22}^{ee^*} \sigma_2\, \chi^{n-1}\, \boldsymbol{\epsilon}^{n-1} \right) , \tag{8}$$

where * denotes the adjoint operation, weight $\eta_{\mathcal{D}}^{n-1}$ and residuals $\boldsymbol{\rho}^{n-1}$ and $\boldsymbol{\epsilon}^{n-1}$ being those associated with the iterates of order $n - 1$ (since one is interested into the gradient of $\mathbf{F}$ at $\mathbf{J}_2^{n-1}$). Accordingly, minimizer α^n of cost functional $\mathbf{F}\left(\mathbf{J}_2^{n-1} + \alpha^n\, \mathbf{v}^n\right)$ for the just determined set of directions $\mathbf{v}^n$ is written in closed form as

$$\alpha^n = \frac{\eta_{\mathcal{S}} \langle \boldsymbol{\rho}^{n-1}, \underline{\mathcal{G}}_{12}^{me}\, \mathbf{v}^n \rangle_{\mathcal{S}} + \eta_{\mathcal{D}}^{n-1} \langle \boldsymbol{\epsilon}^{n-1}, \mathbf{v}^n - \sigma_2\, \chi^{n-1}\, \underline{\mathcal{G}}_{22}^{ee}\, \mathbf{v}^n \rangle_{\mathcal{D}}}{\eta_{\mathcal{S}} \left\| \underline{\mathcal{G}}_{12}^{me}\, \mathbf{v}^n \right\|_{\mathcal{S}}^2 + \eta_{\mathcal{D}}^{n-1} \left\| \mathbf{v}^n - \sigma_2\, \chi^{n-1}\, \underline{\mathcal{G}}_{22}^{ee}\, \mathbf{v}^n \right\|_{\mathcal{D}}^2}. \tag{9}$$

According to the above, contrast source and field are now updated to new values $\mathbf{J}_2^n$ and $\mathbf{E}_2^n = \mathbf{E}_2^{n-1} + \alpha^n\, \underline{\mathcal{G}}_{22}^{ee}\, \mathbf{v}^n$. However, the residual of the *updated* state equation, written as $\boldsymbol{\epsilon} = \sigma_2\, \chi\, \mathbf{E}_2^n - \mathbf{J}_2^n$, valued at $\widetilde{\boldsymbol{\epsilon}}^n$ when the contrast is the present iterate $\chi^{n-1} = \chi_c\, \Psi\left(\tau^{n-1}\right)$, might not be close enough to zero in order to be satisfied with. So, proper updating of the contrast comes by letting $\tau^n = \tau^{n-1} + \beta^n d^n$, where real-valued $\mathbf{r}$-dependent scalar d^n is again of the Polak-Ribière type and where real-valued parameter β^n is a displacement coefficient. For $n > 1$

$$d^n = g^{d,n} + \frac{\langle g^{d,n}, g^{d,n} - g^{d,n-1} \rangle_{\mathcal{D}}}{\langle g^{d,n-1}, g^{d,n-1} \rangle_{\mathcal{D}}} \tag{10}$$

(at $n = 1$, $d^1 = g^{d,1}$). $g^{d,n}$ is the real-valued gradient (Fréchet derivative) at τ^{n-1}, both contrast source $\mathbf{J}_2^n$ and field $\mathbf{E}_2^n$ being now kept fixed, of a weighted-in squared norm $\mathbf{F}_{\mathcal{D}}$ of the above state residual $\boldsymbol{\epsilon}$; in conveniently expanded form, $\mathbf{F}_{\mathcal{D}}$ reads as

$$\mathbf{F}_{\mathcal{D}} = \eta_{\mathcal{D}}^{n-1} \|\sigma_2\, \chi_c\, \Psi\left(\tau\right) \mathbf{E}_2^n - \mathbf{J}_2^n\|_{\mathcal{D}}^2 , \tag{11}$$

where weight $\eta_{\mathcal{D}}^{n-1} = \|\sigma_2\, \chi_c\, \Psi\left(\tau^{n-1}\right) \mathbf{E}_{20}\|_{\mathcal{D}}^{-2}$.

Proceeding as it was the case with the gradient of $\mathbf{F}$ in the above, one can show that

$$g^{d,n} = -2\, \eta_{\mathcal{D}}^{n-1}\, \Psi'\left(\tau^{n-1}\right) \Re\left(\sigma_2\, \chi_c\, \overline{\mathbf{E}_2^n} \cdot \widetilde{\boldsymbol{\epsilon}}^n\right), \tag{12}$$

where Ψ' is the derivative of Ψ with respect to τ, where the upper bar denotes complex conjugation, where $\Re$ denotes the real part, and where residual $\widetilde{\boldsymbol{\epsilon}}^n$ at τ^{n-1} has been defined before; here, $(\,\cdot)$ represents the usual scalar product of (3-component) vectors at given location. (Notice that the weight $\eta_{\mathcal{D}}^{n-1}$ has been kept constant for simplicity, which means that one uses it simply as a normalization factor, and that one is differentiating the factor $\|\sigma_2\, \chi_c\, \Psi\left(\tau\right) \mathbf{E}_2^n - \mathbf{J}_2^n\|_{\mathcal{D}}^2$ only.) As for β^n, the minimizer of $\mathbf{F}_{\mathcal{D}}^n\left(\tau^{n-1} + \beta^n\, d^n\right)$ into the set of directions d^n, it is obtained in closed form as

$$\beta^n = -\frac{\Re\langle d^n\, \sigma_2\, \chi_c\, \Psi'\left(\tau^{n-1}\right) \mathbf{E}_2^n, \widetilde{\boldsymbol{\epsilon}}^n\rangle_{\mathcal{D}}}{\|d^n\, \sigma_2\, \chi_c\, \Psi'\left(\tau^{n-1}\right) \mathbf{E}_2^n\|_{\mathcal{D}}^2}. \tag{13}$$

The algorithm now proceeds by alternating an update of contrast source $\mathbf{J}_2$ via equations (6-9) and an update of contrast τ via equations (10-13) inside each voxel of the prescribed search domain $\mathcal{D}$ until the value reached by the cost functional $\mathbf{F}$ is small enough, or until some plateau is reached. In the latter case, the tuning parameter θ might be reduced in order to push contrast values χ either to 0 or to χ_c, and equivalently to re-distribute voxels into darker ones (at positive τ) and lighter ones (at negative τ), from which the construction of the two sequences is then started again.

3 Numerical results

A number of results has been obtained by the above inversion algorithm. Those shown in figures 2 and 3 consist of gray-level 2-D cross-sectional maps at successive depths (0.1 mm step) of the retrieved 3-D distributions of the contrast χ (after about 2500 iterations, when the cost functional has notably decreased) and of evolution curves of the cost functional $\mathbf{F}$ as a function of the number of iterations.

The example is the one of a 2 mm thick slab of conductivity σ_2 = 1 MS/m where voluminous void defects are sought. A thick circular coil (0.6 and 1.6 mm inner and outer radii, 0.8 mm height) is centered 0.9 mm above the slab at $x = -0.75$ mm and $y = 0$ to avoid undue symmetries with respect to the search domain $\mathcal{D}$ (the latter is centered on the z axis and discretized into $52 \times 52 \times 20$ cubical voxels of $0.1\ \mathrm{mm}^3$ volume). The frequency of operation is 150 kHz, which is corresponding with a plane-wave skin depth δ in metal of about 1.3 mm. One considers in figure 2 and 3 two void parallelepipeds opening in air (the top surface of the slab), both of $1.1 \times 1.1\ \mathrm{mm}^2$ squared horizontal cross-section, the first one 1 mm deep and centered at $x = -1.1\ \mathrm{mm}$, $y = -1.1\ \mathrm{mm}$, the other 0.5 mm deep and symmetrically located at $x = 1.1\ \mathrm{mm}$, $y = 1.1\ \mathrm{mm}$; one considers a single void opening in air in figure 4, which is still of $1.1 \times 1.1\ \mathrm{mm}^2$ squared horizontal cross-section and $1\ \mathrm{mm}$ depth, but its axis is now inclined by $22.5°$.

Data consist of the three components of the anomalous magnetic (Figs. 2-4) or of its single vertical (z) component (Fig. 4) collected at nodes 0.1 mm apart in a planar surface $\mathcal{S}$ of overall area $10\ \mathrm{mm}^2$ and centered $1.55\ \mathrm{mm}$ above $\mathcal{D}$. The inversion is started from a two-level contrast map valued at $\chi = 0.5\, \chi_c$ for the three shallower layers of voxels of $\mathcal{D}$ and at $0.01\, \chi_c$ for the deeper ones, or from a contrast map that evolves with depth as $\chi = 0.5\, \chi_c \exp\left(-z/\delta\right)$

(Fig.4). No refreshment (decrease of θ) has been enforced at this stage of the study, a proper θ having been equated to 1 by numerical experimentation.

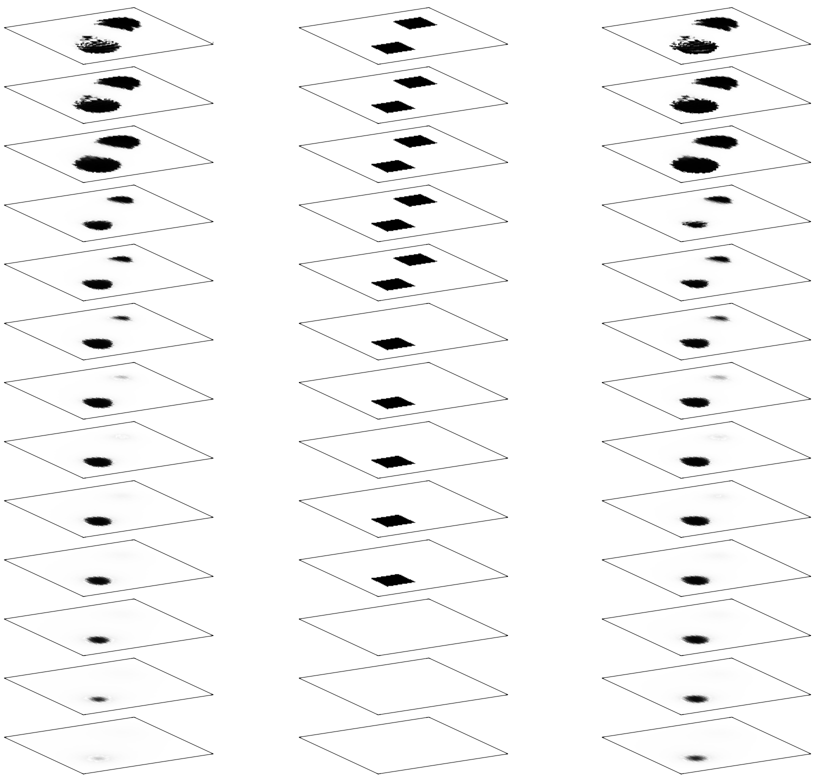

(a) (b) (c)

Figure 2: Retrieval of two voids of different depths in a metal slab (see text for details). Cross-sectional gray-level maps of the conductivity contrast χ at successive 0.1 mm-stepped depths using all three components of the anomalous magnetic field (a), and the vertical component only (c). Exact maps are given in (b) for comparison.

From those results retrievals appear almost identical (and the cost functionals evolve similarly) when all three components of the field are used and when the vertical one is the only one used. This is rather comforting in terms of application to real measurement configurations, e.g., by displacing a small coil probe throughout a plane of observation parallel with the probed metal plate. However, only the shallower parts of the voids, down to about $2/3$ of a skin depth, are fairly well retrieved, the volume of those shallower parts being increased with respect to the exact one and those of the deeper parts being decreased. Such shadowing and blurring due to skin effect are expected phenomena that are faced independently of the inversion algorithm used.

Nevertheless, the results displayed here show that the proposed hybrid technique is rather effective. This is illustrated by the retrieval of two close voids (Fig. 2-3) that appear both fairly located and well discriminated, the inclination of a single one (Fig.4) being well reproduced. Obviously one needs an appropriate initial guess to do so. An initial contrast that exponentially decreases as a function of the depth-to-skin-depth ratio from the usual mid value of $\chi_c/2$, does not lead to a better retrieval than an initial contrast that is set to $\chi_c/2$, in the three first layers of voxels and to almost 0 below (the cost functional reaches a value one-third larger in the first case than in the second case).

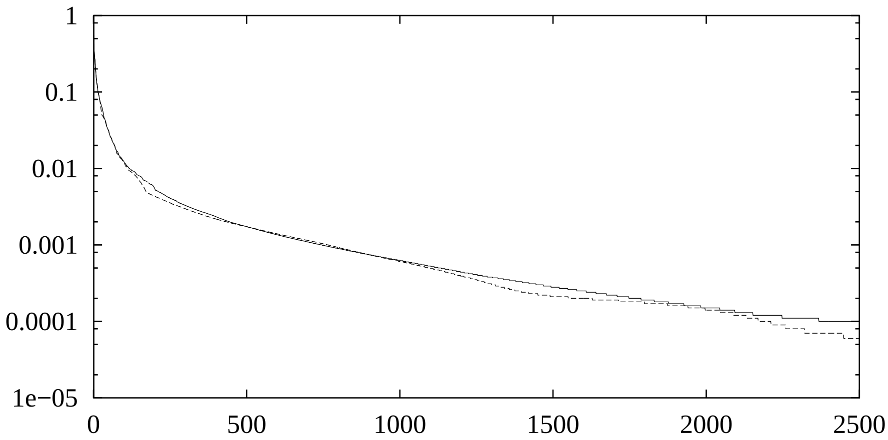

Figure 3: Evolution of the cost functional **F** as a function of the number of iterations for the two voids as studied in Fig. 2. Dotted line, case (c); solid line, case (a).

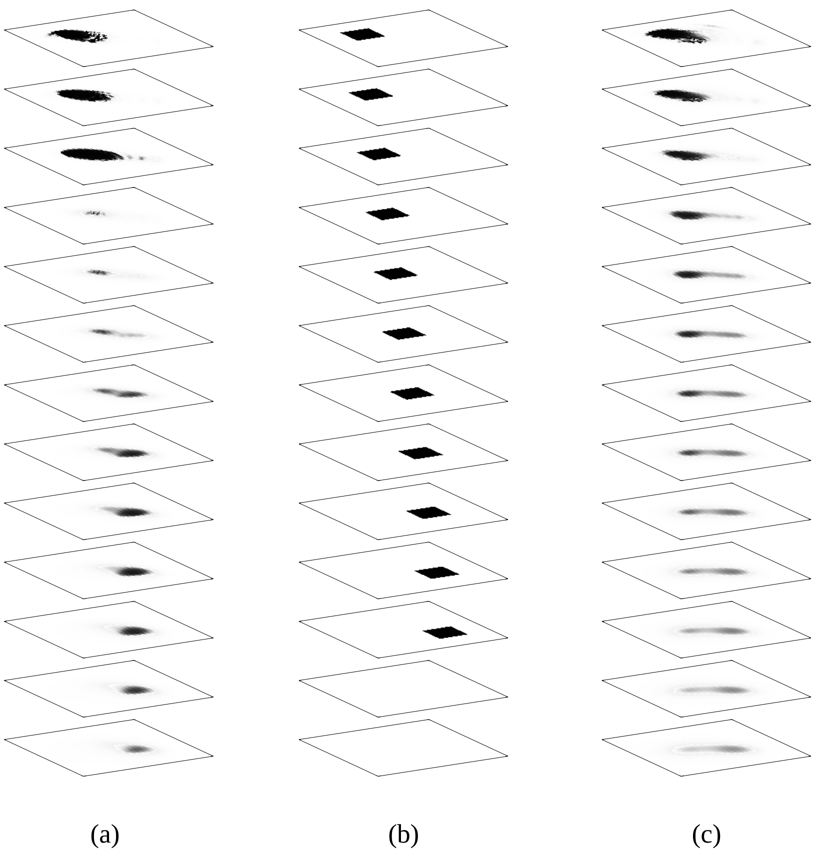

Figure 4: Retrieval of an inclined void in a metal slab (see text for details). Cross-sectional gray-level maps of the conductivity contrast χ at successive 0.1 mm-stepped depths (using all three components of the anomalous magnetic field). The initial contrast χ is chosen as the two-level one in (a), and is chosen as the one exponentially decreasing with depth in (c). Exact maps are given in (b) for comparison.

4 Concluding remarks

So far, data have been assumed to be collected throughout a planar surface (not only along a probing line within a user-prescribed symmetry plane of a defect as is often assumed); this appears to be a pre-requisite when mapping geometrically unknown 3-D objects. Two configurations, other than this multistatic configuration (fixed source – moving field probe), could be attacked similarly, e.g., when source and probe devices are moved together (a reference case would be a SQUID-based magnetometer [7]), or when the variation of the impedance of the probe itself is observed [8]. Work is presently in progress for such two configurations.

However the difficulty in dealing with such new configurations does not lie in the functional analysis, which is carried out as the one sketched here, but in the numerical burden, (one has to construct induced sources for each location of the source device) and in the lack of information (in the second situation, one has to extract pertinent information from a quantity expected to vary more smoothly than the anomalous field).

In addition it remains to study in further detail the influence of the initial guess and of refreshment, and the advantages of frequency-hopping (using data at successive frequencies, from a low one to a high one), whereas the consequence of data noise and model errors should be appraised closely, the synthetic data here having been modeled using the same discretization as the one used in the inversion itself.

References

[1] D. Dos Reis *et al.*, Extended Born domain integral models of diffusive fields, Proc. COMPUMAG'01 Evian, 2001, IV-74-75.

[2] D. Dos Reis *et al.*, On the modeling of 3-D inclusions in conductive media using extended Born models in the diffusive regime, Int. J. Appl. Electromagn. Mechan. (2002) in press.

[3] A. Abubakar and P. M. van den Berg, Three-dimensional inverse scattering applied to cross-well induction sensors, IEEE Trans. Geosci. Remote Sensing 38 (2000) 1669-81.

[4] A. Abubakar *et al.*, A conjugate gradient contrast source technique for 3D profile inversion, IEICE Trans. Electron. E83-C (2000) 1864-1874.

[5] V. Monebhurrun *et al.*, 3-D inversion of eddy current data for Nondestructive Evaluation of steam generator tubes, Inverse Problems 14 (1998) 707-24.

[6] L. Souriau *et al.*, Modified gradient approach to inverse scattering for binary objects in stratified media, Inverse Problems 12 (1996) 463-81.

[7] A. Ruosi *et al.*, High Tc SQUIDS and eddy-current NDE: a comprehensive investigation from real data to modelling, Meas. Sci. Technol. 12 (2000) 1639-48.

[8] T. Takagi *et al.*, ECT research activities in JSAEM Benchmark models of eddy current testing for steam generator tube, Parts 1 and 2. In: R. Collins *et al.* (ed.), Nondestructive Testing of Materials. IOS Press, Amsterdam, 1995, pp. 253-64 and 313-20.